Organic & Biomolecular Chemistry

PAPER

Cite this: *Org. Biomol. Chem.*, 2017, **15**, 7685

Amidinoquinoxaline *N*-oxides: spin trapping of O- and C-centered radicals†

Nadia Gruber,[a,b] Liliana R. Orelli, *[b] Roberto Cipolletti[a] and Pierluigi Stipa *[a]

Received 8th June 2017,
Accepted 23rd August 2017

DOI: 10.1039/c7ob01387f

rsc.li/obc

Amidinoquinoxaline *N*-oxides represent a novel family of heterocyclic spin traps. In this work, their ability to trap O- and C-centered radicals was tested using selected derivatives with different structural modifications. All the studied nitrones were able to trap radicals forming persistent spin adducts, also in the case of OH and OOH radicals which are of wide biological interest as examples of ROS. The stability of the adducts was mainly attributed to the wide delocalization of the unpaired electron over the whole quinoxaline moiety. The nitroxide spectral parameters (hfccs and *g*-factors) were analyzed and the results were supported by DFT calculations. The N-19 hfccs and *g*-factors were characteristic of each aminoxyl and could aid in the identification of the trapped radical. The enhanced stability of the OH adducts under the employed reaction conditions could be ascribed to their possible stabilization by IHBs with two different acceptors: the N–O$^{\bullet}$ moiety or the amidine functionality. DFT calculations indicate that the preferred IHB is strongly conditioned by the amidine ring size. While five membered homologues show a clear preference for the IHB with the N–O$^{\bullet}$ group, in six membered derivatives this stabilizing interaction is preferentially established with the amidine nitrogen as an IHB acceptor.

Introduction

Electron paramagnetic resonance (EPR) spin trapping represents one of the most specific and reliable techniques for detecting and identifying transient free radicals, such as those produced in chemical and biological processes, whose lifetime is too short in the EPR spectroscopic timescale. This technique, widely used since its introduction in the 1970s,[1] is based on the fast reaction between a suitable diamagnetic molecule (a spin trap) and short-lived free radicals with the formation of relatively long-lived radicals (spin adducts), whose EPR signals are persistent enough to be recorded and studied. Additionally, the analysis of hyperfine coupling constants (hfccs) and *g*-factors could aid in the identification of the initially trapped radical.

This technique has been successfully used in biological systems recording a considerable increase in the number of its applications. Many of them are directed toward the study of the role played by Reactive Oxygen Species (ROS) and Oxygen centered Free Radicals (OFRs), such as superoxide, peroxy, hydroperoxy, alkoxy, and hydroxy radicals, with respect to a series of human diseases such as, for example, ischemia-reperfusion syndrome, Friedreich's ataxia, atherosclerosis,[2] neurodegenerative diseases,[3] and cellular aging.[4] In particular, liposoluble spin traps are interesting because they are able to penetrate biological barriers like cell membranes,[5] or to reach the inner layers of the skin.[6]

Nitrones (*N*-oxides) act as very efficient spin traps,[7] being able to undergo fast radical additions with C- and O-centered radicals to yield aminoxyls (nitroxides) as spin adducts, the most persistent organic free radicals in liquid solutions. Among all the commercially available nitrones, *N*-*tert*-butylbenzylideneamine *N*-oxide (PBN) and 5,5-dimethyl-3,4-dihydro-2*H*-pyrrole *N*-oxide (DMPO) are probably the most popular, but their use is not without limitations.[8] For these reasons continuous effort has been devoted to the synthesis of new nitrones[9,10] to be used in spin trapping experiments, with the aim to overcome the typical drawbacks affecting the spin trapping rate, adduct lifetime and the possibility of recognizing the trapped radical from the spectral parameters of the adduct.[11]

Amidinoquinoxaline *N*-oxides represent a heterocyclic core of interest due to their pharmacological properties. Some suit-

[a]*SIMAU Dept. - Chemistry Division, Università Politecnica delle Marche, Via Brecce Bianche 12, Ancona (I-60131), Italy. E-mail: pstipa@univpm.it*
[b]*Departamento de Química Orgánica, Facultad de Farmacia y Bioquímica, Universidad de Buenos Aires. CONICET. Junín 956, (1113) Buenos Aires, Argentina. E-mail: lorelli@ffyb.uba.ar*

† Electronic supplementary information (ESI) available: Scheme for the Synthesis of all nitrones; selected bond distances and dihedral angles for nitrones **1–5**; NMR spectra of compounds **4**, **8**, **9**; cartesian coordinates and thermochemical parameters from frequency calculations of all compounds; selected EPR parameters and Energies and B3LYP/6-31G(d) optimised geometries of isomeric **1b** spin adducts from relaxed PES scan; relative energies and IHB distances and angles for all OH$^{\bullet}$ and OOH$^{\bullet}$ adducts; IHB distances and angles in **3c** and **3e** adducts. See DOI: 10.1039/c7ob01387f

ably substituted derivatives possess antineoplastic activity,[12] especially against hypoxic tumors. Others have been employed as antiamoebic[13] and antianaerobic agents.[14] As part of our research on nitrogen heterocycles, we reported a novel methodology for their synthesis,[15] and investigated some of their chemical,[16] stereochemical[17] and pharmacological[18] properties. In previous work,[19] we studied nitrones derived from the pyrimidoquinoxaline nucleus as novel spin traps, and described their ability to trap methyl radicals produced in a Fenton reaction in DMSO, to yield very persistent nitroxides as spin adducts in the reaction milieu. At the same time, the importance of steric factors has been outlined in such a study: in general, the more hindered nitrones showed lower addition reaction rates, but the corresponding nitroxides decomposed with lower rates too. These features prompted us to investigate their trapping ability toward other radicals including O-centered ones (ROS) due to their relevance in autooxidation processes and in polymers as well as in biological systems. We have also explored the effect of relevant structural modifications in the heterocyclic nitrones.

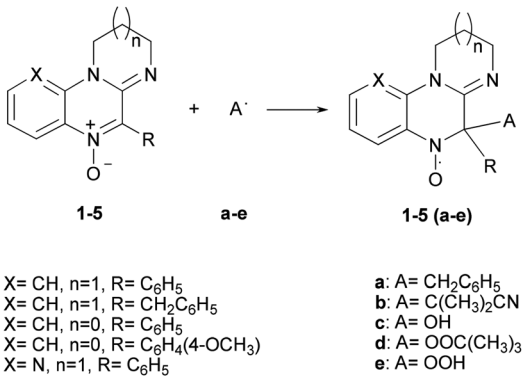

Scheme 1 Spin trapping reactions.

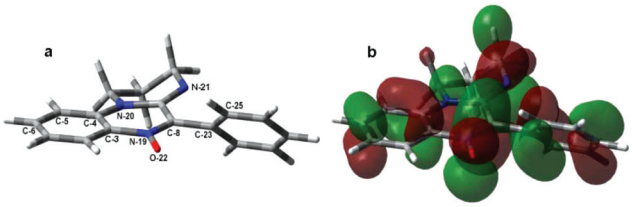

Fig. 1 Tube-type optimized geometry of nitrone **1** computed at the B3LYP/6-31G(d) level (a) showing the arbitrary atom labelling, and HOMO plot (b) computed at the B3LYP/6-31+G(d,p) level: positive values in red and negative in green.

Results and discussion

The studied spin traps, together with the corresponding spin adducts, are reported in Scheme 1. All radical species have been produced in organic solvents as previously reported.[10] Attempts to use other superoxide radical sources were hampered by the water insolubility of the nitrones.‡ In the present study, 2-cyano-2-propyl and benzyl radicals have been chosen as a representative of electrophilic and nucleophilic C-centered radicals, respectively, while hydroxyl, hydroperoxyl and *tert*-butoxyl radicals for ROS. Five model nitrones have been selected, comprising structural variations such as the size of the amidine ring, substitution at the α-carbon and inclusion of an electron withdrawing nitrogen atom in the fused ring.

Compounds **1–5** were obtained as previously reported,[15,19] as well as their computed geometries.[19] As a representative view, the tube-type molecular geometry of **1** computed at the B3LYP/6-31G(d) level, together with the corresponding highest occupied molecular orbital (HOMO) plot, is shown in Fig. 1, showing the arbitrary atom numbering. The oxygen atoms are coloured in red, nitrogen in blue, carbon in grey and hydrogen in white: such a rendering will be used throughout the whole paper. These calculations gave N(19)–C(8) and N(19)–O(22) bond distances of 1.349 (±0.02) and 1.275 (±0.006) Å, respectively, for all nitrones, in good agreement with literature reports.[20] In addition, the N(19)–C(8) double bond is almost coplanar with the aromatic ring of the quinoxaline moiety: the C(8)–N(19)–C(3)–C(4) angle is close to 4° and to 1° for derivatives **1–2** and **3–5**, respectively (data reported in the ESI†). An excellent coplanarity with the above-mentioned ring exists also for N(20): dihedral angles close to 179° are in general formed between N(20), C(4), C(5) and C(6), allowing delocalization of N(20) nonbonding electrons, as shown in the HOMO plot in Fig. 1b. This figure also shows the dihedral angle N(19)–C(8)–C(23)–C(25), which exerts in fact a great influence on the radical addition rates at C(8), mainly ascribed to steric factors.[19] For this reason, in order to study the role played by the attacking radical, those nitrones that do not bear an *ortho*-substituted aromatic ring in that position were chosen for the present study.

All compounds were able to trap the C- and O-centered radicals employed in this study, giving persistent aminoxyls as spin adducts whose EPR signals were detectable for several hours. Although we did not carry out kinetic measurements and our findings are only qualitative, it has to be outlined that in our spin trapping experiments the radicals to be scavenged are not continuously generated. Thus, the persistence of the EPR signals reflects the stability of the adducts.

The EPR parameters (hfccs and *g*-factors) of the adducts are collected in Table 1. For simplicity, only the largest hfccs have been reported with the arbitrary numbering shown in Fig. 2. The experimental values arise from the computer simulation of the corresponding spectra carried out by means of the Winsim program,[21] while the computed ones have been obtained from DFT calculations as previously described.[22] In general, a good agreement between the calculated coupling

‡Attemps of superoxide generation with the xanthine–xanthine oxidase system did not produce any EPR signals due to water insolubility of the nitrones. Neither did the trial in a solvent mixed system using dioxane in a mixture containing 80% (by volume) oxygen-bubbled phosphate buffer (0.1 M, pH 7.3).

Table 1 Selected experimental (exp – in italic) and computed[22] hyperfine coupling constants (hfccs, in Gauss) and *g*-factors of spin adducts **1–5(a–e)** in benzene solution[a,b] according to the arbitrary atom labelling of Fig. 2. The negative sign of the reported experimental values has been attributed on the basis of DFT calculations and was maintained during the optimization process in spectral simulation[e]

Spin adduct	N(19)	H(12)	H(N)(14)	H(13)	H(15)	N(21)	H(16)[c]	H(36)[c]	H–(O)OH	*g*	$\Delta\Delta G^d$
1a,*syn*	11.61	1.18	0.98	−2.96	−2.92	0.51	1.30	0.12		2.00558	5.45
1a,*anti*	9.72	1.10	0.96	−3.06	−3.05	0.19	0.59	0.10		2.00572	
exp	*10.45*	*1.13*	*0.78*	*−3.11*	*−2.86*	*0.40*	*0.47*	*0.20*		*2.00552*	
1b,*syn*	11.66	1.12	0.95	−2.83	−2.83	0.76	1.52	0.21		2.00563	1.66
1b,*anti*	11.33	1.21	1.02	−2.58	−2.55	0.74	0.91	0.40		2.00571	
exp	*10.17*	*1.07*	*0.85*	*−3.02*	*−2.73*	*0.37*	*0.54*	*0.23*		*2.00569*	
1c,*syn*(N–O)	10.70	1.19	1.09	−3.32	−3.39	0.32	1.20	0.17	−0.25	2.00540	1.35
1c,*anti*(N–O)	10.95	1.23	1.10	−3.19	−3.26	0.32	1.05	0.36	−0.24	2.00545	
1c,*syn*(amid)	9.97	1.18	1.00	−2.93	−2.90	0.40	1.22	0.16	−0.18	2.00587	0.31
1c,*anti*(amid)	10.41	1.24	1.00	−2.83	−2.78	0.40	0.94	0.33	−0.39	2.00585	
exp	*10.82*	*1.11*	*0.98*	*−3.01*	*−2.82*	*0.39*	*0.66*	*0.25*	*−0.52*	*2.00548*	
1d,*syn*	10.19	1.12	0.97	−3.01	−3.00	0.32	1.12	0.12		2.00580	1.41
1d,*anti*	9.05	1.03	0.85	−2.59	−2.54	0.77	2.12	0.27		2.00597	
exp	*9.40*	*1.12*	*0.79*	*−3.04*	*−2.68*	*0.43*	*0.48*	*0.19*		*2.00583*	
1e,*syn*(N–O)	11.08	1.16	1.12	−3.31	−3.45	0.30	1.30	0.20	−0.29	2.00541	0.03
1e,*anti*(N–O)	9.58	1.15	0.99	−2.85	−2.85	0.19	0.88	0.26	−0.04	2.00590	
1e,*syn*(amid)	9.68	1.13	0.99	−2.96	−2.95	0.35	1.14	0.20	−0.13	2.00585	2.47
1e,*anti*(amid)	11.33	1.20	1.10	−2.88	−2.95	0.49	0.98	0.39	−0.44	2.00562	
exp	*10.70*	*1.10*	*0.89*	*−2.94*	*−2.79*	*0.39*	*0.67*	*0.24*	*−0.54*	*2.00560*	
2a,*syn*	10.14	1.16	1.03	−3.24	−3.24	0.26	0.68	0.11		2.00555	
2a,*anti*	11.61	1.17	1.00	−3.13	−3.12	0.19	0.48	0.09		2.00563	0.54
exp	*10.23*	*0.91*	*0.75*	*−3.34*	*−3.46*	*0.22*	*0.65*	*0.12*		*2.00547*	
2b,*syn*	10.61	1.15	1.05	−3.00	−3.06	0.31	0.59	0.13		2.00562	1.59
2b,*anti*	10.11	1.16	1.06	−3.22	−3.26	0.22	0.81	0.15		2.00559	
exp	*9.76*	*1.27*	*0.87*	*−2.74*	*−2.99*	*0.48*	*0.49*	*0.22*		*2.00562*	
2c,*syn*(N–O)	10.58	1.14	1.09	−3.20	−3.30	0.37	1.50	0.35	−0.80	2.00545	0.03
2c,*anti*(N–O)	11.02	1.12	1.02	−3.06	−3.10	0.42	1.42	0.34	−0.85	2.00546	
2c,*syn*(amid)	9.74	1.17	1.05	−3.14	−3.14	0.20	0.85	0.23	−0.51	2.00583	3.95
2c,*anti*(amid)	9.52	1.15	1.06	−3.15	−3.16	0.17	0.79	0.17	−0.47	2.00577	
exp	*10.44*	*1.21*	*1.01*	*−3.14*	*−3.29*	*0.40*	*0.88*	*0.23*	*−0.51*	*2.00547*	
2d,*syn*	9.83	1.08	0.91	−2.63	−2.58	0.67	1.57	0.52		2.00580	1.72
2d,*anti*	9.58	0.97	0.89	−2.76	−2.79	0.51	1.74	0.28		2.00576	
exp	*9.47*	*1.14*	*0.79*	*−2.75*	*−3.08*	*0.41*	*0.46*	*0.20*		*2.00569*	
2e,*syn*(N–O)	9.61	1.07	0.90	−2.58	−2.55	0.71	1.63	0.55	0.46	2.00546	2.02
2e,*anti*(N–O)	8.72	1.08	1.02	−2.94	−2.98	0.19	0.97	0.19	−0.43	2.00580	
2e,*syn*(amid)	8.79	1.08	1.00	−2.86	−2.88	0.23	0.78	0.18	−0.37	2.00584	0.37
2e,*anti*(amid)	9.47	1.05	0.99	−3.01	−3.08	0.46	1.82	0.41	0.06	2.00570	
exp	*10.23*	*1.01*	*0.98*	*−3.31*	*−3.42*	*0.39*	*0.89*	*0.17*	*−0.24*	*2.00546*	
3a	11.11	1.12	0.97	−3.11	−3.15	0.32	0.40	0.59		2.00554	—
exp	*10.59*	*0.81*	*0.77*	*−3.08*	*−3.23*	*0.27*	*0.67*	*0.39*		*2.00554*	
3b	11.86	1.08	0.91	−2.74	−2.77	0.57	0.54	1.02		2.00563	—
exp	*10.47*	*0.98*	*0.89*	*−2.88*	*−3.04*	*0.31*	*0.76*	*0.40*		*2.00565*	
3c,(N–O)	10.72	1.14	1.04	−3.18	−3.29	0.40	0.68	0.98	−0.30	2.00543	1.50
3c,(amid)	9.87	1.16	0.98	−2.97	−2.95	0.35	0.76	0.57	−0.49	2.00578	
exp	*10.77*	*1.09*	*0.86*	*−2.82*	*−3.00*	*0.34*	*0.60*	*0.24*	*−0.55*	*2.00552*	
3d	9.00	0.95	0.83	−2.63	−2.62	0.73	1.49	1.21		2.00592	—
exp	*9.55*	*1.10*	*1.00*	*−2.76*	*−2.91*	*0.30*	*0.70*	*0.29*		*2.00571*	
3e,(N–O)	11.04	1.11	1.02	−2.92	−3.03	0.51	1.14	0.68	−0.40	2.00559	0.12
3e,(amid)	9.65	1.10	0.96	−2.89	−2.91	0.37	0.62	0.81	−0.13	2.00584	
exp	*10.68*	*1.01*	*0.89*	*−2.75*	*−2.86*	*0.22*	*0.68*	*0.32*	*−0.36*	*2.00557*	
4a	11.39	1.15	0.95	−2.87	−2.85	0.48	0.86	0.40		2.00563	—
exp	*10.41*	*0.87*	*0.775*	*−3.06*	*−3.14*	*0.27*	*0.66*	*0.43*		*2.00554*	
4b	11.51	1.13	0.93	−2.28	−2.70	0.49	0.40	0.87		2.00567	—
exp	*9.98*	*1.21*	*0.89*	*−3.014*	*−2.886*	*0.24*	*0.73*	*0.49*		*2.00576*	
4c,(N–O)	10.68	1.14	1.03	−3.20	−3.29	0.38	0.93	0.64	−0.30	2.00543	1.71
4c,(amid)	10.14	1.14	0.95	−2.88	−2.87	0.38	0.84	0.48	−0.16	2.00587	
exp	*10.67*	*1.00*	*0.84*	*−2.67*	*−2.86*	*0.34*	*0.65*	*0.48*	*−0.55*	*2.00548*	
4d	8.98	0.96	0.83	−2.64	−2.62	0.73	1.48	1.20		2.00579	—
exp	*9.76*	*1.17*	*1.04*	*−2.65*	*−2.78*	*0.40*	*0.97*	*0.70*		*2.00569*	
4e,(N–O)	10.74	1.06	1.05	−3.13	−3.33	0.61	1.41	1.25	−1.57	2.00539	0.78
4e,(amid)	9.69	1.10	0.95	−2.91	−2.92	0.36	0.77	0.57	−0.12	2.00583	
exp	*10.89*	*0.926*	*0.78*	*−3.1*	*−3.19*	*0.48*	*0.72*	*0.29*	*−0.58*	*2.00553*	
5a,*syn*	11.34	1.14	−0.78	−3.27	−3.31	0.46	1.18	0.15		2.00555	0.22
5a,*anti*	10.96	1.15	−0.78	−3.18	−3.22	0.59	0.81	0.44		2.00570	
Exp	*10.22*	*1.02*	*0.86*	*−3.62*	*−3.79*	*0.24*	*0.70*	*0.34*		*2.00553*	

Table 1 *(Contd.)*

Spin adduct	N(19)	H(12)	H(N)(14)	H(13)	H(15)	N(21)	H(16)[c]	H(36)[c]	H–(O)OH	*g*	$\Delta\Delta G$[d]
5b,*syn*	11.44	1.08	−0.75	−3.09	−3.17	0.71	1.42	0.25		2.00561	5.45
5b,*anti*	9.28	1.13	−0.85	−3.42	−3.51	0.18	0.78	0.24		2.00569	
exp	*10.85*	*1.08*	*−0.78*	*−2.92*	*−3.42*	*0.62*	*1.53*	*1.533*		*2.00561*	
5c,*syn*(N–O)	10.04	0.99	−0.77	−3.19	−3.28	0.49	1.75	0.46	−0.83	2.00586	2.32
5c,*anti*(N–O)	10.12	1.16	−0.89	−3.67	−3.84	0.25	1.17	0.25	−0.29	2.00546	
5c,*syn*(amid)	9.68	1.18	−0.83	−3.24	−3.29	0.32	0.89	0.37	−0.41	2.00579	0.42
5c,*anti*(amid)	9.71	1.15	−0.80	−3.21	−3.26	0.36	1.12	0.18	−0.20	2.00583	
exp	*10.31*	*1.28*	*−0.81*	*−3.15*	*−3.55*	*0.55*	*1.13*	*0.55*	*−0.32*	*2.00543*	
5d,*syn*	9.85	1.09	−0.80	−3.36	−3.43	0.27	1.08	0.18		2.00578	1.21
5d,*anti*	8.95	1.00	−0.68	−2.85	−2.86	0.74	2.07	0.36		2.00595	
exp	*9.21*	*1.11*	*−0.99*	*−2.91*	*−3.33*	*0.36*	*0.70*	*0.50*		*2.00617*	
5e,*syn*(N–O)	*10.71*	*1.11*	*−0.82*	*−3.29*	*−3.45*	*0.48*	*0.99*	*0.49*	*−0.40*	*2.00543*	*0.26*
5e,*anti*(N–O)	10.63	1.12	−0.83	−3.34	−3.51	0.44	1.33	0.23	−0.41	2.00555	
5e,*syn*(amid)	8.68	1.09	−0.84	−3.20	−3.29	0.19	0.92	0.37	−0.07	2.00583	2.33
5e,*anti*(amid)	9.44	1.11	−0.81	−3.26	−3.32	0.33	1.10	0.24	−0.12	2.00583	
exp	*10.70*	*1.02*	*−0.57*	*−2.79*	*−2.79*	*0.10*	*0.72*	*0.28*	*−0.29*	*2.00554*	

[a] Dioxane for OH trapping. [b] Improved spectral resolution after dilution with acetonitrile for benzyl adducts. [c] H(16) and H(36) are nonequivalent; hence their hfccs are different. [d] Differences in Reaction Gibbs Free Energy ($\Delta\Delta G$, in kcal mol^{-1}) between couples of isomers computed at the M062X/6-31+G(d,p) level. [e] Spectral simulations were carried out by means of the Winsim program.[21]

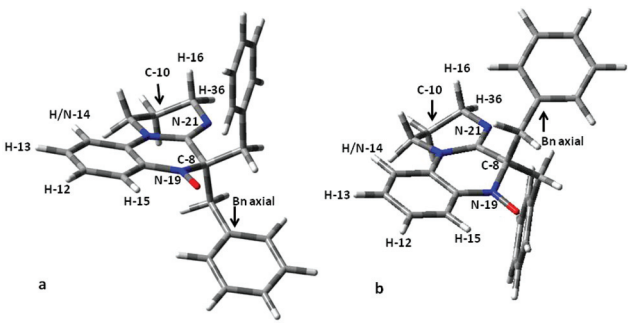

Fig. 2 Tube-type B3LYP/6-31G(d) optimised structures for spin adducts **2a**: the axial benzyl substituent is located on the same (a) or on the opposite face (b) of C(10) methylene, named *syn* and *anti*, respectively.

constants and the experimental ones was found. In the case of superoxide trapping, only the replacement of $OO^{\bullet}$- with $HOO^{\bullet}$ in the corresponding DFT calculations gave hfcc values in satisfactory agreement with the experimental results. This implies that protonation could in some way occur in the reaction medium, as suggested for the corresponding DMPO analogue.[23] For nitroxides arising from nitrones **1**, **2** and **5**, in which the amidine function is part of a tetrahydropyrimidine ring, two minima were found in all cases. Their geometries were labelled as "*syn*" and "*anti*" when methylene C(10) (amidine ring) and substituent R at C(8) (Scheme 1) are located on the same or on the opposite face, respectively. Aminoxyl **2a**, which represents the only achiral adduct, shows two minima corresponding to the axial benzyl substituent located on the same (Fig. 2a – *syn*) or opposite face (Fig. 2b – *anti*) as methylene C(10).

Finally, adducts derived from OH and OOH radicals (**1–5c** and **1–5e**) represent a special case, and their geometries will be treated separately in this paper. Aminoxyls **1**, **2**, and **5** show in fact four energy minima, arising from the relative disposition of the substituent R at C8 (Scheme 1) with respect to C-10 (*syn*, *anti*) and from the formation of Intramolecular Hydrogen Bonds (IHBs) with O(22) of the N–O$^{\bullet}$ moiety, or with the amidine nitrogen N(21). Two energy minima were located for adducts derived from nitrones **3**, **4**, corresponding to IHBs with both possible acceptors.

Data reported in Table 1 show that the EPR spectra recorded are characteristic of the trapped radical. These spectra were interpreted, and hence simulated, on the basis of hfccs typical of this kind of radical, in which the nitrogen three lines are mainly split by two different couples of aromatic hydrogens of the quinoxaline moiety: H(13) and H(15) with the larger hfccs (*ca.* 3 Gauss) and H(12) and H(14) with the smaller ones (*ca.* 1 Gauss). In addition, the splitting of the two non-equivalent protons H(16) and H(36) is clearly visible, while a further splitting of *ca.* 0.4 Gauss was assigned to N(21). In aminoxyls from nitrone **5**, the H(14) splitting is replaced by the N(14) one, while in the 5-membered amidine derivatives **3** and **4** further couplings, attributable to the two remaining methylenic protons of the amidine ring, are observed on the basis of DFT calculations (data not shown). These results could be easily explained considering a wide delocalization of the unpaired electron over the whole quinoxaline moiety, in line with what observed in indolinonic[22] and benzoxazinic nitroxides:[10] as a typical example, in Fig. 3 the SOMO (a) and Spin density (b) distribution plots for compound **1d** have been reported. Fig. 3a clearly shows the SOMO marked π-character and the unpaired electron delocalization. Fig. 3b displays the negative spin densities found for H(13) and H(15), justifying the negative sign of the corresponding hfcc values. Moreover, this figure clearly shows the relatively large spin density values observed on N(21), explaining its relatively large hfcc; similarly, the relatively large spin density found on the substituent oxygen atoms could explain why

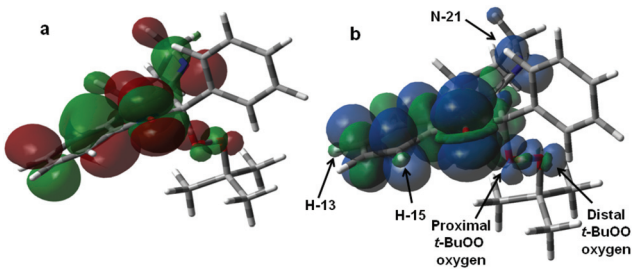

Fig. 3 Single occupied molecular orbital (SOMO) (a) and α–β spin density distributions (b) of **1d** computed at the unrestricted B3LYP/EPR-III level. Positive spin densities are in red (a) and blue (b), while negative ones are always in green. Spin densities on H(13), H(15), and N(21) and on the *t*-BuOO oxygens are indicated by arrows (see text).

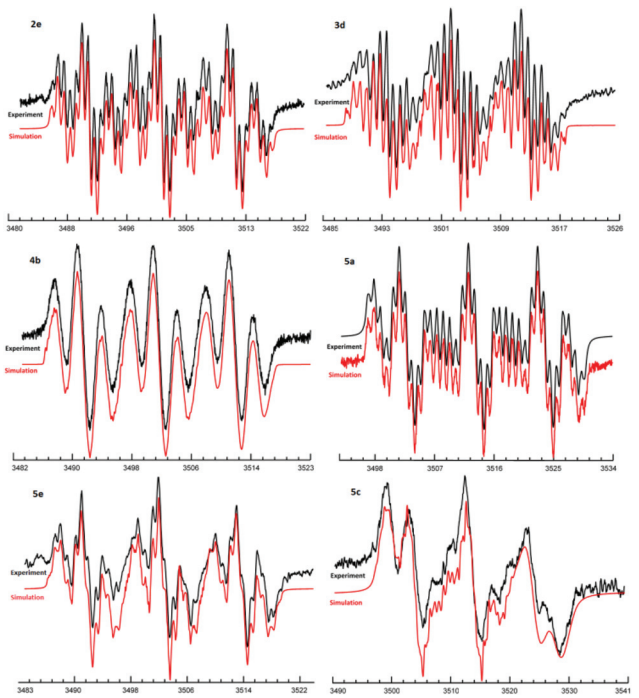

Fig. 4 Experimental (upper trace) and simulated (lower trace) EPR spectra of selected spin adducts.

aminoxyls **1**–**5d** show the smallest N(19) hfccs of the series. Finally, in Fig. 4 the experimental EPR spectra of some adducts, together with the corresponding simulations, are shown as typical examples.

Since EPR parameters are very sensitive to geometry, their DFT computation was performed taking into account the possibility of different geometries (*syn* and *anti*), as mentioned before. However, a comparison of these data with the experimental ones does not allow the establishment of the predominant isomer. In addition, proper frequency calculations at the M062X/6-31+G(d,p) level[24] upon the corresponding B3LYP/6-31G(d) optimised geometries show, besides very few examples (**1a** and **5b**), quite small energy differences ($\Delta\Delta G$ in Table 1) between pairs of isomers, suggesting that the recorded spectra should be considered as a dynamic average of their signals.

In order to gain a deeper insight into the possible structures arising from radical scavenging, proper relaxed (*i.e.* with geometry optimization at each step) Potential Energy Surface (PES) scans at the B3LYP/6-31G(d) level have been performed. In these studies, the possible contribution of the substituents at C(8) due to steric factors has also been considered. As a typical example, different conformations of aminoxyl **1b**,***syn*** chosen for the relative bulkiness of the 2-cyano-2-propyl group have been investigated. The results indicate the presence of 6 minima (Fig. 5), showing that the C(8)-phenyl substituent always prefers the axial orientation, and that the energy differences among the resulting minima are extremely small. A typical plot resulting from a simultaneous relaxed PES scan of both C(7)–C(8)–C(23)–C(25) and N(19)–C(8)–C(37)–C(46) dihedral angles is shown in Fig. 5 (optimised geometries and calculations reported in the ESI†).

Concerning nitrogen hyperfine coupling in aminoxyls, it is worth recalling that its value is determined by spin density on the atom and by hybridization. Spin density is mainly located on the N–O$^{\bullet}$ group[25] with typical values for alkyl aminoxyls of about 14–15 G but, if conjugation with an aromatic system is possible, the corresponding hfccs are somewhat smaller due to spin delocalization.[26] This is the case for N(19) hyperfine couplings determined for the aromatic aminoxyls obtained in the present work, ranging from 9.21 (**5d**) to 10.89 G (**4e**), as well as for other aromatic aminoxyls described in the literature.[22,26,27] Regarding N(19) hybridization, its pyramidalization degree (Table 4 ESI†) indicates a planar geometry (sp^2), showing no significant variation among the individual geometries.

N(19) hfccs may also be affected by the nature of the radical added to the *α*-carbon C(8), since it may contribute both to the unpaired electron delocalization and to the geometry of the whole system. In particular, geometric factors such as bond distances and out of plane angles[10] could influence the value of nitrogen hyperfine coupling. Data reported in Table 1 indicate a variation in N(19) hfccs depending on the trapped radical, with the highest values for HO$^{\bullet}$ and HOO$^{\bullet}$ adducts

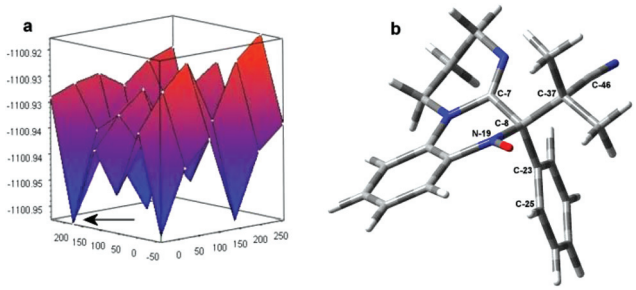

Fig. 5 (a) **1b**,***syn*** plot of relaxed PES simultaneous scan of C(7)–C(8)–C(23)–C(25) and N(19)–C(8)–C(37)–C(46) dihedral angles at the B3LYP/6-31G(d) level; the arrow indicates isomer **1b**,***syn*-1**, whose molecular geometry is shown in (b) (details in the ESI†).

(**1–5c** and **1–5e**, respectively) and the lowest ones for *tert*-butoxyl radicals (spin adducts **1–5d**). From the above discussion, it arises that analysis of aminoxyl N-coupling could be a useful approach for the identification of the species trapped by these nitrones.

Moreover, in organic free radicals the isotropic *g*-factor deviates from the corresponding value of the free electron (2.0023) due to spin–orbit coupling effects arising from the contribution of each individual atom. As a consequence, the contribution of a specific group results from all its atoms, and will be larger the more the odd electron is delocalized onto that group, producing the corresponding deviation of *g* from the free electron value. These substituent shifts of *g* in π-type radicals (including aminoxyls) are quite characteristic of the radical structure.[28] Analysis of data collected in Table 1 reveals that *g* changes with the trapped radical, the maximum values being usually found for **1–5d**, where the *tert*-butoxyl group participates in the delocalization of the unpaired electron, as previously stated and as shown in Fig. 3. This last finding represents another important feature of the studied nitrones, because the *g*-value estimation of a spin adduct together with N(19) hfccs and with the specific pattern of the EPR spectrum could represent an aid for the identification of the trapped radical. A plot of the experimental values of N(19) hfccs *versus* *g*-factors for all detected spin-adduct indicates a possible relationship between aminoxyl nitrogen coupling and the *g*-value for each radical trapped (Fig. 6): higher *g*-factors are associated with smaller N(19)-hfccs.

As previously mentioned, aminoxyls derived from our nitrones are stabilized by delocalization of the unpaired electron in the π-system, and show unusual persistence in organic solvents presumably due to the absence of hydrogens α- to the *N*-oxide function.[19] Additionally, in hydroxyl and hydroperoxyl adducts, the possibility of Intramolecular Hydrogen Bond (IHB) formation could contribute to stabilization. Such interactions had also been proposed in alcoxyamine derived nitroxides[29] and in benzoxazinic analogues originating from OH$^{\bullet}$ radical trapping,[30] in which unexpectedly high hfccs (0.5–0.7 Gauss) were found for the –OH proton, with an increase of the nitroxide nitrogen coupling as well.§ Accordingly, the EPR spectra of aminoxyls **1–5c**, but also those derived from OOH radical trapping (**1–5e**), showed the highest N(19) couplings of the series, together with others of about 0.5 Gauss attributable to the –OH or –OOH proton (Table 1), thus reinforcing our hypothesis. Furthermore, our system has another potential H bond acceptor, represented by the amidine nitrogen N(21): these possibilities could contribute to adduct stabilization, accounting for their enhanced persistence in organic solvents, as for derivatives **1–5e**, which showed no appreciable decrease of the EPR signal intensity after several hours.

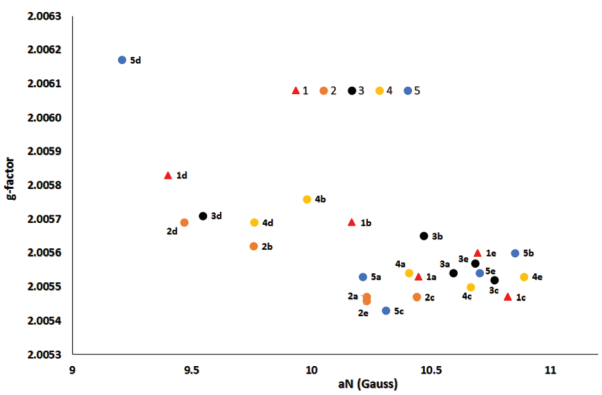

Fig. 6 Experimental N-19 hfcc (a^N) *versus* *g*-factor plot for adducts **1–5 (a–e)**.

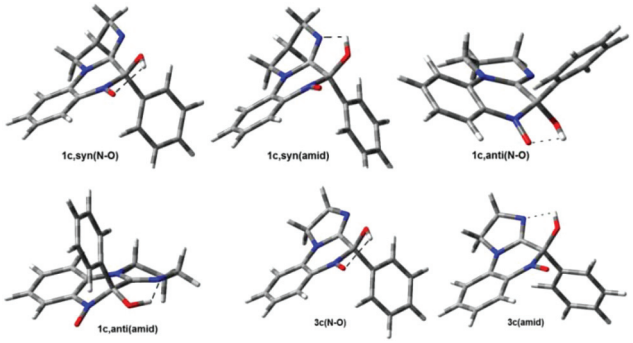

Fig. 7 B3LYP/6-31G(d) optimized geometries of **1c** and **3c**. Dotted lines indicate possible IHBs.

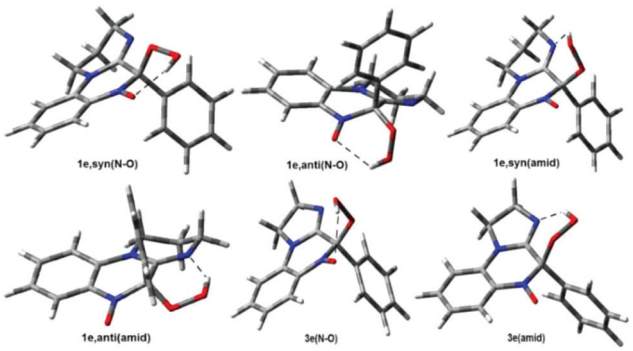

Fig. 8 B3LYP/6-31G(d) optimized geometries of **1e** and **3e**. Dotted lines indicate possible IHBs.

Both possibilities to yield IHBs were studied by DFT calculations (details in the Experimental section) upon OH and OOH radical adducts from nitrones **1–5**. Four energy minima were located for adducts arising from nitrones **1**, **2** and **5** and two for those arising from nitrones **3** and **4**. The resulting optimized geometries of **1e** and **3e** (OOH$^{\bullet}$ adducts) and of **1c** and **3c** (OH$^{\bullet}$ adducts) are reported in Fig. 7 and 8 as typical examples, labelled as *syn*/*anti* as already described, and as "N–O" or "amid" depending on the two possible IHBs.

§ Nitroxides have two different resonance structures. Hydrogen bonding stabilizes the zwitterionic structure, which leads to an increase of aN.[29]

Table 2 IHB distances (in Ångström, Å), IHB angles (in degrees, °), Reaction Gibbs free energies (ΔG) and activation Gibbs free energies ($\Delta G^{\#}$) for OH (**1c** and **3c**) and OOH (**1e** and **3e**) spin adducts

Nitroxide geometry	ΔG (kcal mol^{-1})	$\Delta G^{\#}$ (kcal mol^{-1})	IHB distance	IHB angle
1c,*anti*(N–O)	−44.79	6.09	2.04	114
1c,*anti*(amid)	−46.46	7.05	1.93	123
1c,*syn*(N–O)	−46.14	6.62	2.04	115
1c,*syn*(amid)	−46.77	6.62	1.92	123
1e,*anti*(N–O)	−16.63	14.59	2.10	123
1e,*anti*(amid)	−15.29	17.28	1.85	139
1e,*syn*(N–O)	−16.66	16.49	1.89	136
1e,*syn*(amid)	−17.76	16.08	2.04	127
3c,(N–O)	−43.87	5.75	2.09	112
3c,(amid)	−42.37	6.30	2.11	119
3e,(N–O)	−15.00	14.34	2.15	122
3e,(amid)	−14.88	16.26	1.91	138

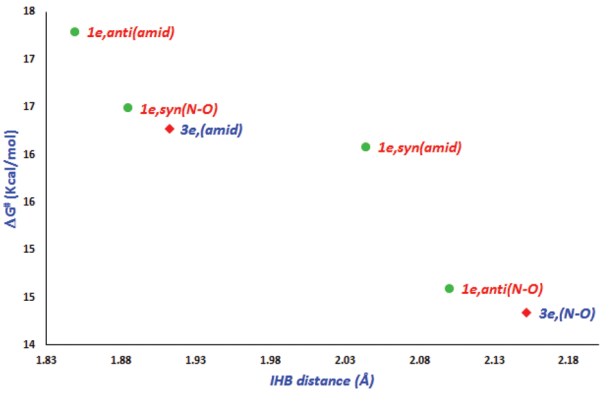

Fig. 9 Computed Gibbs free energies (kcal mol^{-1}) of activation *vs.* IHB distances for OOH$^{\bullet}$ spin adducts of nitrones **1** and **3**.

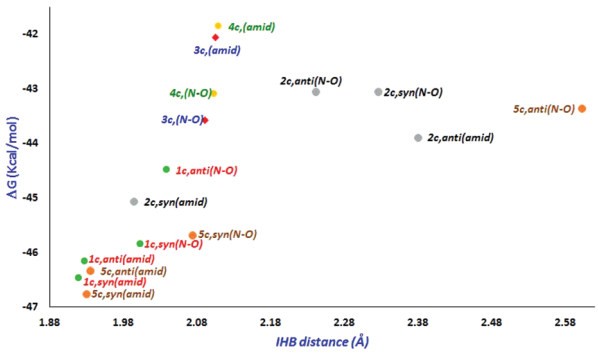

Fig. 10 Computed Gibbs free energies (kcal mol^{-1}) *vs.* IHB distances for OH$^{\bullet}$ adducts of nitrones **1**–**5**.

Since the possibility of an IHB could affect the spin adduct properties, their bond distances and O–H···O or O–H···N angles (Fig. 8 ESI†) for "N–O" or "amid" isomers, respectively, have been considered as an indication of the corresponding strength.[31] In particular, their possible correlation with adduct stabilities, estimated from the corresponding computed reaction Gibbs Free Energy changes (ΔG), has been investigated. In addition, the possibility of different formation rates has been considered by computing the corresponding Activation Gibbs Free Energies ($\Delta G^{\#}$). Results obtained for representative derivatives **1c,e** and **3c,e** are collected in Table 2.

In line with the results previously obtained with benzoxazine nitrones,[32] the energies involved in the spin trapping reactions show significantly more negative values for OH$^{\bullet}$ adduct formation with respect to OOH$^{\bullet}$ trapping, in which the IHB brings about the formation of a 6-membered ring. The reported values indicate that **1e,*syn*(amid)** represents the most stable structure for OOH radical addition to nitrone **1**, despite its much longer IHB distance and smaller angle with respect to the corresponding ***anti*** analogue which, in turn, is less stable. In addition, no significant energy differences were found between the two remaining isomers, in which the N–O$^{\bullet}$ moiety is involved in the IHB, regardless of the corresponding differences found in bond distances and angles. In fact, the structure with the best IHB distance and angle (**1e,*anti*(amid)**) is less stable. It could therefore be concluded that the possibility of hydrogen bonding in these nitroxides does not play by itself a dominant role in their stabilisation, which is mainly determined by the extensive delocalization of the unpaired electron.[19] The same analysis of the remaining OOH$^{\bullet}$ adducts is in line with these results (Table 3 ESI†). In addition, by comparing the corresponding activation parameters, it appears that shorter IHB distances decrease OOH radical addition rates (Fig. 9), suggesting that IHB formation should not be a relevant stabilizing factor in the corresponding transition states as well.

On the other hand, as the OH radical trapping is concerned, IHB formation proceeds always through a 5-membered ring formation. Although no clear correlation between computed activation parameters and IHB distances has been found in this case, the reaction Gibbs Free Energies (ΔG) correlate in general well with IHB distances (Fig. 10) and angles (Table 3 ESI†), outlining the importance of such interaction in adduct stabilisation. It is noteworthy that an IHB with the amidine moiety is preferred in the additions to nitrones **1**, **2** and **5**, while adducts derived from **3** and **4** show the opposite behaviour. This amidine ring size effect could be a consequence of the different basicity of both amidine moieties, which in turn reflects their ability as H bond acceptors. In fact, it has been reported[33] that 1,2-diaryltetrahydropyrimidines are considerably more basic than the homologous imidazolines.¶ It is known that the basic site in cyclic amidines is the formally sp^2 nitrogen, acting in our case as the IHB acceptor. Hence, nitroxides with more basic amidine nitrogens would preferentially establish IHBs with this function.

In summary, IHBs would be a relevant stabilizing factor only in the case of OH$^{\bullet}$ adducts. Besides, a change in the preferential IHB interaction with the size of the amidine ring is observed: while the five membered homologues **3** and **4** show a clear preference for the IHB with the N–O$^{\bullet}$ functionality, in

¶Reported pK_a values for 1-phenyl-2-(4-nitrophenyl)imidazoline: 7.65 and for 1-phenyl-2-(4-nitrophenyl)-1,4,5,6-tetrahydropyrimidine: 10.51 (from ref. 33).

the six membered ones an IHB involving the amidine nitrogen would be preferred.

Conclusions

Amidinoquinoxaline nitrones are able to trap O- and C-centered radicals to form persistent nitroxides. Their stabilization could be at least in part attributed to the wide delocalization of the unpaired electron over the whole π-system. In the case of $OH^{\bullet}$ adducts, DFT calculations indicate that additional stabilization in organic solvents would result from IHB interaction between the trapped radical and the N–$O^{\bullet}$ moiety or the amidine nitrogen. The preferred IHB is strongly conditioned by the amidine ring size, suggesting that there is a determinant difference in the basicity of the amidine nitrogens that define their ability as IHB acceptors. Besides, the N-19 hfccs and *g*-factors are characteristic of each nitroxide and could contribute, together with the specific pattern of the EPR spectrum, to the identification of the radical trapped.

In summary, the high persistence of the spin adducts in organic solvents, including those derived from ROS, together with the possibility of identifying the radical trapped by means of their EPR spectral parameters makes these new spin traps of potential interest for their applications in other chemical or suitable biological systems.

Experimental

Melting points were determined with a Büchi capillary apparatus and are uncorrected. ^{1}H and ^{13}C NMR spectra were recorded on a Bruker Bio Spin Avance III 600 MHz spectrometer, a Bruker Avance II 500 MHz spectrometer or a Bruker MSL 300 MHz spectrometer, using deuterochloroform as the solvent. Chemical shifts are reported in parts per million (ppm) relative to TMS as an internal standard. Coupling constants are reported in Hz. D_2O was employed to confirm exchangeable protons (ex). Splitting multiplicities are reported as singlet (s), broad signal (bs), doublet (d), double doublet (dd), doublet of double doublets (ddd), and multiplet (m). HRMS (ESI) was performed with a Bruker MicroTOF-Q II spectrometer. Reagents, solvents, and starting materials were purchased from standard sources and purified according to literature procedures.

Synthesis of *N*-oxides 1–5. General procedure

***N*-Oxides 1–5 were prepared by cyclodehydration of aminoamides 6–10 (Scheme 1 and ESI†).**[15] A mixture of the aminoamide (1 mmol) and ethyl polyphosphate (PPE, 1 mL/0.05 g) was refluxed for 5 h in an oil bath. After reaching room temperature, the resulting solution was extracted with water (5 × 6 mL). The aqueous phases were pooled, filtered and made alkaline with 10% aqueous NaOH. The mixture was extracted with chloroform (3 × 15 mL). The organic phases were washed with water, dried over sodium sulphate and filtered. The chloroformic solution was left at r.t. until no further conversion to compounds **1–5** was evidenced by TLC (silica gel, chloroform : methanol 9 : 1). The solvent was then removed *in vacuo* and the crude product was purified by column chromatography (silica gel, chloroform : methanol 10 : 0–9 : 1).

Compounds **1**, **2**,[15] **3**[34] and **5**[19] are described in the literature. Yield and analytical data of compound **4** are as follows.

4-(4-Methoxyphenyl)-1,2-dihydroimidazo[1,2-*a*]quinoxaline 5-oxide 4. This compound was obtained as an orange solid (0.208, 71%), mp 168–170 °C (from EtOH). ^{1}H NMR (600 MHz, $CDCl_3$, TMS): δ 8.28 (1H, dd, J = 8.4, 1.4), 7.97 (2H, d, J = 8.9), 7.45 (1H, ddd, J = 8.1, 7.3, 1.4), 7.10 (1H, ddd, J = 8.4, 7.3, 1.2), 6.99 (2H, d, J = 8.9), 6.79 (1H, dd, J = 8.1, 1.2), 4.16–4.21 (2H, m), 4.03–4.08 (2H, m), 3.85 (3H, s). ^{13}C NMR (151 MHz, $CDCl_3$): δ 161.0, 153.1, 135.8, 133.2, 132.2, 131.9, 131.2, 121.4, 121.3, 120.7, 113.5, 111.9, 55.5, 54.2, 46.7. HRMS (ESI) m/z: $[M + H]^+$ calcd for $C_{17}H_{16}N_3O_2$: 294.1237. Found: 294.1231.

Synthesis of *N*-arylacetyl-*N*′-(2-nitroaryl)-1,3-propanediamines and *N*-arylacetyl-*N*′-(2-nitroaryl)-1,2-ethanediamines 6–10. General procedure

Acyl chloride (1 mmol) was added to a chloroformic solution of the corresponding *N*-(*o*-nitrophenyl)-1,*n*-diamine (1 mmol in 15 mL), followed by 4% NaOH aqueous solution (1 mL). The mixture was shaken for 15 min, after which the organic layer was separated, washed with H_2O, dried (Na_2SO_4) and filtered. The solvent was removed *in vacuo*. The crude product was purified by flash chromatography on silica gel using mixtures of chloroform : ethyl acetate as the eluent.

Compounds **6**, **7**,[15] and **10**[19] are described in the literature. Yields and analytical data of new compounds are as follows.

***N*-Phenylacetyl-*N*′-(2-nitrophenyl)ethylenediamine 8.** This compound was obtained as an orange solid (0.224 g, 75%), mp 77–79 °C (from hexane/chloroform). ^{1}H NMR (500 MHz, $CDCl_3$): δ 8.14 (1H, d, J = 8.6), 7.39–7.44 (1H, m), 7.27–7.33 (3H, m), 7.18–7.22 (2H, m), 6.92 (1H, d, J = 8.6), 6.63–6.68 (1H, m), 5.90 (1H, bs ex), 3.58 (2H, s), 3.44–3.50 (4H, m). ^{13}C NMR (125 MHz, $CDCl_3$): δ 172.1, 145.4, 136.5, 134.5, 129.54, 129.47, 129.2, 127.6, 127.0, 115.9, 113.8, 43.7, 42.0, 39.0. HRMS (ESI) m/z: $[M + H]^+$ calcd for $C_{16}H_{18}N_3O_3$: 300.1343. Found: 300.1332.

***N*-(4-Methoxyphenyl)acetyl-*N*′-(2-nitrophenyl)ethylenediamine 9.** This compound was obtained as an orange solid (0.237 g, 72%), mp 95–97 °C (from hexane/chloroform). ^{1}H NMR (300 MHz, $CDCl_3$): δ 8.15 (1H, dd, J = 8.6, 1.7), 8.08 (1H, bs ex), 7.43 (1H, ddd, J = 8.6, 6.9, 1.7), 7.11 (2H, d, J = 8.6), 6.93 (1H, d, J = 8.6), 6.84 (2H, d, J = 8.6), 6.66 (1H, ddd, J = 8.6, 6.9, 1.2), 5.87 (1H, bs ex), 3.78 (3H, s), 3.52 (2H, s), 3.44–3.50 (4H, m). ^{13}C NMR (75 MHz, $CDCl_3$) δ 172.4, 159.0, 145.4, 136.5, 132.2, 130.6, 127.0, 126.5, 115.8, 114.6, 113.8, 55.4, 42.9, 42.1, 39.0. HRMS (ESI) m/z: $[M + H]^+$ calcd for $C_{17}H_{20}N_3O_4$: 330.1448. Found: 330.1453.

EPR measurements

Isotropic X-band EPR spectra were recorded on a Bruker EMX spectrometer system equipped with a microwave frequency

counter and an NMR Gaussmeter for field calibration; for *g*-factor determination the whole system was standardized with a sample of perylene radical cations in concentrated sulfuric acid (g = 2.00258). General EPR spectrometer settings: microwave power 5 mW, modulation amplitude 0.2 Gauss, time constant 0.64 ms, receiver gain 4.48×10^4, sweep time 1342.177 s, and conversion time 1310.720 ms. EPR spectra simulations were carried out by means of the Winsim program, freely available from NIEHS.[21] EPR spectral parameters for all nitroxide spin adducts are collected in Table 1.

Spin trapping experiments

Spin trapping experiments were performed by generating the radical to be trapped directly in the sample tube in the presence of the nitrone under investigation in argon deaerated benzene (0.1 mM) solutions. A different solvent was used in the trapping of HO radicals in the Fenton system: aqueous $FeSO_4$ (10 μM) was added to a [1,4]dioxane degassed solution of the nitrone (0.1 mM) in the presence of 20 μM hydrogen peroxide. EPR spectra were recorded 40 s after the addition of $FeSO_4$. A 10 μM benzene solution of potassium superoxide (KO_2) was used as source of superoxide anions prepared by adding the minimum amount of 18-crown-6 necessary to ensure complete solubility of KO_2 in benzene. *tert*-Butylperoxyl radicals were generated by adding traces of solid lead dioxide (PbO_2) to a degassed benzene solution containing 0.1 mM of the nitrone and 10 μM of a commercially available *tert*-butylhydroperoxide nonane solution. Benzyl radicals were produced by *in situ* PbO_2 oxidation of the corresponding Grignard reagent from commercial ethereal solutions as previously described.[35] 2-Cyano-2-propyl radicals were generated by thermal decomposition of 2,2′-azobisisobutyronitrile (AIBN), added as a solid to the starting nitrone solution.

Computational details

Density Functional Theory[36] calculations were carried out using the Gaussian 09 suite of programs[37] on the GALILEO cluster at Cineca Supercomputing Center.[38] The spin adduct (nitroxides) conformations were systematically screened by means of appropriate relaxed (*i.e.*, with optimization at each point) Potential Energy Surface (PES) Scans at the B3LYP/6-31G(d) level to ensure that species were global minimum energy structures. In particular, in the study upon **1b** conformers, a 360° relaxed PES scan was performed simultaneously of the C(7)–C(8)–C(23)–C(25) and N(19)–C(8)–C(37)–C(46) dihedral angles at the same time at the B3LYP/6-31G(d) level. Each conformer characterized by a relative Energy minimum was subjected to a further optimization without constraints. In addition, the geometry optimization of all aminoxyls was carried out with the unrestricted formalism, giving $\langle S^2 \rangle$ = 0.7501 ± 0.0003 for spin contamination (after annihilation). Moreover, in frequency calculations on all conformers characterized by an Energy minimum in the corresponding PES, imaginary (negative) values were never found, confirming that the computed geometries were always referred to a minimum. Thermodynamic quantities were computed at 298 K by means of frequency calculations performed by employing the M06-2X[24] functional in conjunction with the 6-31+G(d,p) basis set. EPR parameter calculations were performed following the multistep procedure previously described.[22] Transition state optimizations were performed employing the MPW1K functional[39] in conjunction with the 6-31G(d) basis set for optimizations and 6-31+G(d,p) for frequency calculations; in these last runs, all optimized stationary points were found to have the appropriate number of imaginary frequencies, and the imaginary modes (negative sign) correspond to the correct reaction coordinates, also confirmed by their visualization with appropriate programs.

Conflicts of interest

There are no conflicts to declare.

Acknowledgements

Università Politecnica delle Marche and University of Buenos Aires (UBACyT 20020130100466BA) are kindly acknowledged for financial support, as well as Cineca Supercomputing Center for Computational Resource Allocation (ISCRA grant ANTIOX-D, code: HP10CZ6SCE).

Notes and references

1 (*a*) A. Mackor, Th. A. J. W. Wajer and Th. J. de Boer, *Tetrahedron Lett.*, 1966, **40**, 2115; (*b*) M. Iwamura and N. Inamoto, *Bull. Chem. Soc. Jpn.*, 1967, **40**, 702; (*c*) G. R. Chalfont, M. J. Perkins and A. Horsfield, *J. Am. Chem. Soc.*, 1968, **90**, 7141; (*d*) E. G. Janzen and B. J. Blackburn, *J. Am. Chem. Soc.*, 1968, **90**, 5909; (*e*) C. Lagerscrantz and S. Forshult, *Nature*, 1968, **218**, 1247.

2 J. A. Berliner and J. W. Heinecke, *Free Radical Biol. Med.*, 1996, **20**, 707.

3 (*a*) R. T. Dean, S. Fu, R. Stocker and M. J. Davies, *Biochem. J.*, 1997, **324**, 1; (*b*) S. Fu, M. J. Davies, R. Stocker and R. T. Dean, *Biochem. J.*, 1998, **333**, 519.

4 (*a*) J. Moskovitz, M. B. Yim and P. B. Chock, *Arch. Biochem. Biophys.*, 2002, **397**, 354; (*b*) R. A. Floyd and K. Hensley, *Neurobiol. Aging*, 2002, **23**, 795.

5 A. Iannone, A. Marconi, G. Zambruno, A. Giannetti, V. Vannini and A. Tomas, *J. Invest. Dermatol.*, 1993, **101**, 59.

6 A. Ribier, Q. L. Nguyen, J.-T. Simonnet and B. Boussouira, *US* 5569663A, 1996.

7 (*a*) E. G. Janzen, *Acc. Chem. Res.*, 1971, **4**, 31; (*b*) C. A. Evans, *Aldrichimica Acta*, 1979, **12**, 23; (*c*) C. Mottley and R. P. Mason, in *Biological Magnetic Resonance 8*, ed. L. J. Berliner and J. Reuben, Plenum Publishers, New York, 1989, p. 489; (*d*) P. Tordo, *Electron Paramagn. Reson.*, 1998, **16**, 116; (*e*) G. R. Buettner, *Free*

Radical Biol. Med., 1987, **3**, 259; (*f*) E. G. Janzen and J. I.-P. Liu, *J. Magn. Reson.*, 1973, **9**, 510; (*g*) E. G. Janzen, C. A. Evans and J. I.-P. Liu, *J. Magn. Reson.*, 1973, **9**, 513; (*h*) E. G. Janzen, in *Free Radicals in Biology*, ed. W. Prior, Academic Press, New York, 1980, p. 115.

8 (*a*) Y. Kotake and E. G. Janzen, *J. Am. Chem. Soc.*, 1991, **113**, 9503; (*b*) K. Makino, T. Hagiwara, H. Imaishi, M. Nishi, S. Fuji, H. Ohya and A. Murakami, *Free Radical Res. Commun.*, 1990, **9**, 233; (*c*) E. Finkelstein, G. M. Rosen and E. Rauckman, *Mol. Pharmacol.*, 1982, **21**, 262.

9 (*a*) R. D. Hinton and E. G. Janzen, *J. Org. Chem.*, 1992, **57**, 2646; (*b*) A. Zeghdaoui, B. Tuccio, J.-P. Finet, V. Cerri and P. Tordo, *J. Chem. Soc., Perkin Trans. 1*, 1995, 2087; (*c*) E. G. Janzen, Y. K. Zhang and D. L. Haire, *Magn. Reson. Chem.*, 1994, **32**, 711; (*d*) C. Fréjaville, H. Karoui, B. Tuccio, F. Le Moigne, M. Culcasi, S. Pietri, R. Lauricella and P. Tordo, *J. Chem. Soc., Chem. Commun.*, 1994, 1793; (*e*) C. Fréjaville, H. Karoui, B. Tuccio, F. Le Moigne, M. Culcasi, S. Pietri, R. Lauricella and P. Tordo, *J. Med. Chem.*, 1995, **38**, 258; (*f*) K. Stolze, N. Udilova and H. Nohl, *Biol. Chem.*, 2002, **383**, 813; (*g*) K. Stolze, N. Udilova, T. Rosenau, A. Hofinger and H. Nohl, *Biol. Chem.*, 2003, **384**, 493; (*h*) H. Zhao, J. Joseph, H. Zhang, H. Karoui and B. Kalyanaraman, *Free Radicals Biol. Med.*, 2001, **31**, 599; (*i*) G. Olive, A. Mercier, F. Le Moigne, A. Rockenbauer and P. Tordo, *Free Radicals Biol. Med.*, 2000, **28**, 403; (*j*) P. Tsai, S. Pou, R. Straus and G. M. Rosen, *J. Chem. Soc., Perkin Trans. 2*, 1999, 1759; (*k*) G. M. Rosen, P. Tsai, E. D. Barth, G. Dorey, P. Casara, M. Spedding and H. J. Halpern, *J. Org. Chem.*, 2000, **65**, 4460.

10 P. Astolfi, M. Marini and P. Stipa, *J. Org. Chem.*, 2007, **72**, 8677. For a review see: R. Improta and V. Barone, *Chem. Rev.*, 2004, **104**, 1231.

11 O. Ouari, M. Hardy, H. Karoui and P. Tordo, *Electron Paramagn. Reson.*, 2011, **22**, 1.

12 G. E. Adams, E. M. Fielden, M. A. Naylor and I. J. Stratford, *UK Pat. Appl. GB* 2257360, 1993.

13 P. C. Parthasarathy, B. S. Joshi, M. R. Chaphekar, D. H. Gawad, L. Anandan, M. A. Likhate, M. Hendi, S. Mudaliar, S. Iyer, D. K. Ray and V. B. Srivastava, *Indian J. Chem., Sect. B: Org. Chem. Incl. Med. Chem.*, 1983, **22**, 1250.

14 (*a*) G. J. Ellames, K. R. Lawson, A. A. Jaxa-Chamiec and R. M. Upton, *EP* 0256545, 1988; (*b*) G. J. Ellames and A. A. Jaxa-Chamiec, *US Pat* 4696928, 1987; (*c*) G. J. Ellames, R. M. Upton, A. A. Jaxa-Chamiec and P. L. Myers, *US Pat* 4761414, 1988.

15 M. B. García, L. R. Orelli, M. L. Magri and I. A. Perillo, *Synthesis*, 2002, 2687.

16 M. B. Garcia, L. R. Orelli and I. A. Perillo, *J. Heterocycl. Chem.*, 2006, **43**, 1703.

17 J. E. Díaz, N. Vanthuyne, H. Rispaud, C. Roussel, D. Vega and L. R. Orelli, *J. Org. Chem.*, 2015, **6**, 1689.

18 M. L. Lavaggi, G. Aguirre, L. Boiani, L. R. Orelli, B. García, H. Cerecetto and M. González, *Eur. J. Med. Chem.*, 2008, **43**, 1737.

19 N. Gruber, L. L. Piehl, E. Rubin de Celis, J. E. Díaz, M. B. García, P. Stipa and L. R. Orelli, *RSC Adv.*, 2015, **5**, 2724.

20 (*a*) F. A. Villamena, C. M. Hadad and J. L. Zweier, *J. Am. Chem. Soc.*, 2004, **126**, 1816; (*b*) F. Villamena, M. H. Dickman and D. R. Crist, *Inorg. Chem.*, 1998, **37**, 1446; (*c*) J. C. A. Boeyens and G. J. Kruger, *Acta Crystallogr., Sect. B: Struct. Crystallogr. Cryst. Chem.*, 1970, **26**, 668; (*d*) Y. K. Xu, Z. W. Chen, J. Sun, K. Liu, W. Chen, W. Shi, H. M. Wang, X. K. Zhang and Y. Liu, *J. Org. Chem.*, 2002, **67**, 7624.

21 D. Duling, *PEST Winsim (Version 0.96)*, National Institute of Environmental Health Sciences, Triangle Park, NC, 1996.

22 P. Stipa, *Chem. Phys.*, 2006, **323**, 501.

23 F. A. Villamena, J. K. Merle, C. M. Hadad and J. L. Zweier, *J. Phys. Chem. A*, 2005, **109**, 6083.

24 Y. Zhao and D. G. Truhlar, *Theor. Chem. Acc.*, 2008, **120**, 215.

25 (*a*) A. Di Matteo, C. Adamo, M. Cossi, V. Barone and P. Rey, *Chem. Phys. Lett.*, 1999, **310**, 159; (*b*) A. Di Matteo, C. Adamo, V. Barone and P. Rey, *J. Phys. Chem.*, 1999, **103**, 3481; (*c*) A. Di Matteo, A. Bencini, M. Cossi, V. Barone, M. Mattesini and F. Totti, *J. Am. Chem. Soc.*, 1998, **120**, 7069; (*d*) V. Barone, A. Grand, D. Luneau, P. Rey, C. Minichino and R. Subra, *New J. Chem.*, 1993, **17**, 545; (*e*) J. Cirujeda, J. Vidal-Gancedo, O. Jürgens, F. Mota, J. J. Novoa, C. Rovira and J. Veciana, *J. Am. Chem. Soc.*, 2000, **122**, 11393; (*f*) A. Zheludev, V. Barone, M. Bonnet, B. Delley, A. Grand, E. Ressouche, P. Rey, R. Subra and J. Schweizer, *J. Am. Chem. Soc.*, 1994, **116**, 2019; (*g*) S. M. Mattar and A. L. Stephens, *Chem. Phys. Lett.*, 2000, **319**, 601.

26 M. Beyer, J. Fritscher, E. Feresin and O. Schiemann, *J. Org. Chem.*, 2003, **68**, 2209.

27 C. Berti, M. Colonna, L. Greci and L. Marchetti, *Tetrahedron*, 1975, **31**, 1745.

28 H. Fischer, in *Free Radicals*, ed. J. K. Kochi, Wiley-Interscience, New York, 1973, Vol. II, p. 435.

29 S. Marque, H. Fischer, E. Baier and A. Studer, *J. Org. Chem.*, 2001, **66**, 1146.

30 P. Stipa, *Tetrahedron*, 2013, **69**, 4591.

31 E. Arunan, G. R. Desiraju, R. A. Klein, J. Sadlej, S. Scheiner, I. Alkorta, D. C. Clary, R. H. Crabtree, J. J. Dannenberg, P. Hobza, H. G. Kjaergaard, A. C. Legon, B. Mennucci and D. J. Nesbitt, *Pure Appl. Chem.*, 2011, **83**, 1637.

32 P. Astolfi, P. Carloni, M. G. Marini, G. Mobbili, M. Pisani and P. Stipa, *RSC Adv.*, 2013, **3**, 22023.

33 I. Perillo, B. Fernandez and S. Lamdan, *J. Chem. Soc., Perkin Trans. 2*, 1977, 2068.

34 N. A. Isley, R. T. H. Linstadt, S. M. Kelly, F. Gallou and B. H. Lipshutz, *Org. Lett.*, 2015, **17**(19), 4734.

35 P. Stipa, L. Greci, P. Carloni and E. Damiani, *Polym. Degrad. Stab.*, 1997, **55**, 323.

36 (*a*) R. G. Parr and W. Yang, *Density Functional Theory of Atoms and Molecules*, Oxford University, New York, NY,

1998; (*b*) W. Koch and M. C. Holthausen, *A Chemist's Guide to Density Functional Theory*, Wiley-VCH, Weinheim, Germany, 2000.
37 M. J. Frisch, *et al.*, *Gaussian 09 (Revision D.01)*, Gaussian Inc., Wallingford, CT, 2009.
38 Cineca Supercomputing Center, *via* Magnanelli 6/3, I-40033 Casalecchio di Reno, Bologna, Italy, http://www.cineca.it/HPSystems.
39 B. J. Lynch, P. L. Fast, M. Harris and D. G. Truhlar, *J. Phys. Chem. A*, 2000, **104**, 481.